Relativistic R-matrix calculations of photoionization cross sections for Na-like Cr^{13+} ions

Juqiang Wang and Zhongwen Wu †

Key Laboratory of Atomic and Molecular Physics and Functional Materials of Gansu Province, College of Physics and Electronic Engineering, Northwest Normal University, Lanzhou 730070, China

E-mail: zhongwen.wu@nwnu.edu.cn

June 2026

Abstract. The direct and resonant photoionization processes of Na-like Cr^{13+} ions from the ground state $1s^22s^22p^63s\ ^2S_{1/2}$ and two lowly excited $1s^22s^22p^63p\ ^2P_{1/2,\,3/2}$ states are explored by means of relativistic R-matrix calculations. Particular emphasis is placed on analysis of resonance structures and determination of direct and resonant ionization limits. For this purpose, we calculated the energy levels of Cr^{13+} and adjacent Cr^{14+} ions, together with the photoionization cross sections over a wide photon energy range on a fine grid. The obtained ionization limits are found to be in good accordance with the NIST values. For the ground state, 25 well-resolved resonance peaks are identified, with their respective total angular momentum and parity determined. By comparing the energy levels with the resonance positions extracted from the cross sections, these resonances are assigned to the double-excitation channels $1s^22s^22p^53lnl'$ ($l = p, d$). In contrast, for the two excited states, only the direct ionization limits can be reliably determined. Owing to high density and complexity of the resonance structures, individual resonances and their corresponding resonant ionization limits cannot be unambiguously identified. This work provides a comprehensive set of photoionization cross-section data for Na-like Cr^{13+} ions, filling a critical gap in direct and resonant photoionization studies and offering valuable support for diagnostic analysis and numerical modeling of chromium-containing astrophysical and laboratory plasmas. In addition, the photoionization dataset supporting the present findings is publicly retrievable from the Science Data Bank at https://www.scidb.cn/s/JFjQnm (https://doi.org/10.57760/sciencedb.j00113.00331).

Keywords: photoionization, Na-like Cr^{13+} ions, ionization limits, resonance structure

1. Introduction

Photoionization is an essential atomic mechanism that occurs in a wide range of environments, including astrophysical plasmas [1–4], laboratory plasmas [5, 6], stellar atmospheres [7–10], and the Earth's upper atmosphere [11–13]. In astrophysics, accurate photoionization data are crucial for spectral modeling of stellar atmospheres, interstellar medium, and nebulae, being the fundamental basis of quantifying elemental abundances across the cosmos as well as of analyzing stellar chemical evolution pathways [14–17]. In laboratory plasma physics, these data provide essential support for plasma diagnostics in magnetic and inertial confinement fusion devices, as well as for characterizing laser-produced plasmas [18–20]. Furthermore, photoionization cross sections and relevant atomic parameters serve as reliable benchmarks for studying complex many-electron dynamics, such as electron correlation and relativistic interactions [21–24].

Chromium (Cr), a member of the iron-group elements [25, 26], possesses atomic data of high relevance to both astrophysics [27–29] and fusion research [30–32]. The cosmic abundances of transition metals from scandium to nickel ($21 \leq Z \leq 28$) exhibit a characteristic "peak" structure around iron [33–35]. As a representative element of this group, photoionization cross sections and radiative transition probabilities of Cr are fundamental for analyzing late-type stellar spectra and performing non-local thermodynamic equilibrium modeling of astrophysical plasmas [35–37]. Beyond astrophysics, chromium serves as a major constituent of stainless steel, a widely used structural material in fusion devices such as tokamaks [38, 39]. Consequently, chromium ions widely exist as impurities within fusion plasmas, and their atomic properties directly affect the precision of plasma diagnostics as well as the evaluation of key plasma properties such as electron density, temperature, and ionization balance [40, 41]. A particularly important class of ions for these studies is the Na-like isoelectronic sequence. These ions possess a simple closed-shell structure with a single valence electron, making them ideal systems for atomic structure calculations and for probing fundamental atomic processes [42–44]. Highly charged Na-like ions are abundant in various high-temperature plasma environments. Their relatively simple spectral structure makes them exceptionally suitable for applications ranging from plasma diagnostics and X-ray laser development to L-shell diagnostics in fusion plasmas [45–50].

Existing research on the photoionization of chromium has primarily focused on neutral Cr and its lowly charged ions [51–54]. Early studies successfully identified Cr spectral signatures in the interstellar medium and performed preliminary calculations of photoionization cross sections for several low-ionization stages [55–58]. However, systematic studies on highly ionized chromium ions remain scarce. Despite some recent progress [59, 60], a comprehensive theoretical investigation into the direct

and resonant photoionization processes of highly ionized Cr^{13+} is still lacking. To fill this gap, we conduct a systematic investigation into the photoionization of Na-like Cr^{13+} ions by employing the fully relativistic R-matrix approach together with the multiconfigurational Dirac-Hartree-Fock (MCDHF) method, which provides a comprehensive set of photoionization data for the first time. These results, together with other relevant datasets, are expected to be used for stellar spectral modeling, fusion plasma diagnostics, and broader understanding of dynamical effects in highly charged iron-group ions [61–63].

The remainder of this contribution is organized as follows. Section 2 reviews the core components of the theoretical method adopted in this work, together with relevant computational details. Section 3 presents and analyzes the obtained photoionization results, with particular emphasis upon the cross sections, resonance structure, and direct ionization limits. Finally, this work is summarized briefly in Section 4.

2. Theoretical method and computational details

2.1. Overview of the relativistic R-matrix theory

The present study is based primarily on the relativistic R-matrix theory and the MCDHF method. As the MCDHF framework has been elaborated extensively in prior literature (see, e.g., Ref. [64]), the present overview is confined just to the essentials of the R-matrix theory. Wigner and coworkers originally proposed the foundational R-matrix framework in 1947 for nuclear physics research [65]. Beginning in 1971, Burke *et al.* developed the non-relativistic R-matrix method and its associated computational code particularly for atomic physics [66]. In 1975, Chang [67] developed an improved version of the R-matrix package based on the GRASP program, which was successfully applied to heavy-ion calculations. In 2004, Norrington *et al.* [68] released the fully relativistic Dirac Atomic R-matrix Code (DARC), which has been widely used in studies of various processes such as electron impact excitation and photoionization. For example, we studied the photoionization of Si^{2+}, Ca^{7+}, and W^{63+} ions by means of the DARC package [69–71].

The R-matrix theory is built on the central ideology of partitioning the scattering space into both inner and outer regions by a sphere of radius a. Within this theoretical framework, the continuum electron and the target ion possessing N electrons form an $(N+1)$-electron scattering system. The inner region (i.e., with $r < a$) is treated as an $(N+1)$-electron system, analogous to a bound state, with its wave function given by a configuration-interaction wave function, constructed as described in Ref. [68],

$$\Psi_k^{N+1} = \sum_{ij} c_{ijk} \hat{A}[\Phi_i^N, u_{ij}]^{J\pi} + \sum_q d_{qk} \theta_q^{N+1} \,. \tag{1}$$

Here, the symbol $\hat{A}[\Phi_i^N, u_{ij}]^{J\pi}$ stands for the coupled wave function of the composite $(N+1)$-electron system. It is explicitly constructed by coupling the target-ion wave function $\Phi_i^N \equiv |J_i^t \, \pi_i^t\rangle$ (describing the N-electron system after photoionization) with the continuum-orbital one of the photoelectron, $u_{ij} \equiv |\varepsilon\kappa m\rangle$, in which the quantities ε, κ, and m denote its kinetic energy, Dirac quantum number, and magnetic quantum number. The antisymmetrization operator $\hat{A}$ enforces the antisymmetry of the coupled wave function upon exchanging the bound and continuum electrons. θ_q^{N+1} denotes the correlation function that characterizes bound channels formed as a continuum electron attaches to the N-electron target ion, thereby preserving wave function orthonormality and completeness (1). Both the expansion coefficients c_{ijk} and d_{qk} are determined via the diagonalization of the Dirac Hamiltonian matrix for the $(N+1)$-electron system using variational methods. The indices i, j, and k label the channels, continuum-orbital basis functions, and eigenvectors, respectively.

In the outer region (i.e., with $r > a$), the continuum electron can be considered to move in the target-ion Coulomb potential, with its continuum-orbital wave function obtained from asymptotic expansion or perturbative approximation. Ultimately, by integrating the theoretical treatments for the inner and outer regions, the corresponding R-matrix and K-matrix, as well as the desired photoionization cross sections, can be obtained [72]. Specifically, under the electric-dipole (E1) approximation, one would write the photoionization cross sections as follows with the use of the wave function $\Psi_{j\varepsilon}^-$ of the composite $(N+1)$-electron system and the one Ψ_i of the initial target ion [68],

$$\sigma = \frac{8\pi^2 \alpha C}{3(2J_i+1)} \sum_{ljJ} |\langle \Psi_{j\varepsilon}^- \| \hat{D}_1 \| \Psi_i \rangle|^2 \,. \tag{2}$$

Here, $\hat{D}_1$ is the E1 operator of radiation fields. The superscript "–" on $\Psi_{j\varepsilon}^-$ indicates that it has the asymptotic form of a Coulomb-modified plane wave. J_i is the total angular momentum of the initial state of the target ion, while l and j are the orbital and total angular momenta of the photoelectron, respectively. α is the fine structure constant. For the length gauge, the constant C is set to be ω, whereas $C = 1/\omega$ applies to the calculations within the velocity gauge.

2.2. Computational details and data acquisition

As non-dipole contributions of the ionizing light field have been known just to exert negligible influence on atomic photoionization by light covering the infrared to soft x-ray

range [73], all the calculations are carried out here under the E1 approximation. Energy levels and wave functions of Cr^{14+} ions are calculated with the GRASP2K package, which implements the MCDHF approach. The convergence of the calculated energy levels, wave functions, and photoionization cross sections is tested by considering five configuration models including principal quantum numbers up to $n = 3$, 4, 5, 6, and 7, yielding 37, 75, 113, 151, and 189 fine-structure energy levels, respectively. The model with $n = 3$ already shows reasonable convergence. Nonetheless, to ensure reliable structure and photoionization data, the present calculations adopt the configuration model including principal quantum number up to $n = 4$, consisting of 11 configurations and 16 Dirac orbitals. By means of the ORBS, INTS, NJGRAF, DSTGH, and PDSTG3 components of the DARC package, we compute in sequence the continuum-orbital bases, radial integrals, angular integrals, Hamiltonian diagonalization, and the photoionization cross sections on the basis of the obtained formatted "TARGET.INP" file. As far as the present DARC calculations are concerned, a fine energy grid of 10^{-4} Ryd is adopted, yielding 8×10^5 photon energy points to sufficiently describe the photoionization cross sections in the energy regime considered. Because of the fine energy grid, the narrow resonance peaks associated with inner-shell excitations can be resolved from the photoionization cross sections. Furthermore, 30 continuum orbitals per angular momentum are employed, which satisfies the recommended minimum of 20 continuum orbitals for heavy atoms [74] and is well within the range commonly adopted in similar R-matrix photoionization studies [75–77]. Within the present configuration model, the radius of the R-matrix sphere is fixed at $a = 4.44$ a.u., being large enough to incorporate all required orbitals, thereby ensuring a complete set of orbital bases. This value is comparable to the radii adopted in R-matrix photoionization calculations for other Na-like and Mg-like ions [75, 76], supporting the validity of the present choice. For the resonant photoionization from the ground state [Ne]$3s$ $(J)^\pi = (1/2)^e$ (channel number $n_\mathrm{c} = 138$; Hamiltonian size $n_\mathrm{H} = 4259$) of Cr^{13+} ions considered here, just two combinations of total angular momentum J and parity π are allowable for the doubly-excited intermediate states following the preceding photoexcitation, namely, $(J)^\pi = (1/2)^o$ ($n_\mathrm{c} = 139$; $n_\mathrm{H} = 4288$) and $(J)^\pi = (3/2)^o$ ($n_\mathrm{c} = 241$; $n_\mathrm{H} = 7415$).

3. Results and discussion

Table 1 tabulates some of the lowly excited energy levels of Cr^{14+} ions obtained in this work by using three computational schemes, i.e., DARC, Flexible Atomic Code (FAC) [79], and GRASP2K [80]. The DARC and GRASP2K calculations adopt the same configurations consisting of $1s^22s^22p^6$, $1s^22s^22p^5nl$ (n = 3–4), and $1s^22s2p^6nl$ ($n = 3$), while the FAC calculation uses a broader set of configurations

Table 1: Lowly excited energy levels (in eV) of Cr^{14+} ions computed using three different computational schemes (i.e., the DARC, MCDHF, and FAC), compared with the NIST reference values. $\Delta\% = |\text{MCDHF} - \text{NIST}|/\text{NIST} \times 100\%$.

Index	Configuration	$^{2S+1}L_J$	DARC	MCDHF	FAC	NIST [78]	$\Delta\%$
1	$2s^22p^6$	$^1S_0$	0.00	0.00	0.00	0.00	
2	$2s^22p^53s$	$^3P_1$	584.23	584.04	584.69	586.14	0.36
3	$2s^22p^53s$	$^3P_0$	591.47	591.08	591.60	593.1620	0.35
4	$2s^22p^53s$	$^1P_1$	592.64	592.22	592.89	594.28	0.35
5	$2s^22p^53p$	$^3S_1$	608.99	608.84	609.42	610.7994	0.32
6	$2s^22p^53p$	$^1S_0$	620.06	619.84	620.86	621.7266	0.30
7	$2s^22p^53p$	$^3P_1$	614.51	614.37	615.31	616.2803	0.31
8	$2s^22p^53p$	$^3D_1$	621.00	620.65	621.58	622.5173	0.30
9	$2s^22p^53p$	$^1P_1$	623.33	622.98	623.91	624.8768	0.30
10	$2s^22p^53p$	$^3P_0$	638.45	638.29	639.56	637.7271	0.09
11	$2s^22p^53d$	$^3P_0$	649.47	649.33	650.06	651.3445	0.31
12	$2s^22p^53d$	$^3P_1$	650.27	650.08	650.83	652.0848	0.31
13	$2s^22p^53d$	$^3D_1$	658.81	658.57	659.39	660.12	0.24
14	$2s^22p^53d$	$^1P_1$	669.78	669.37	670.21	670.30	0.14
15	$2s^12p^63s$	$^1S_0$	709.38	709.21	709.68	712.82	0.51
16	$2s^12p^63p$	$^3P_1$	732.77	732.74	733.12	730.82	0.26
17	$2s^12p^63p$	$^1P_1$	736.06	735.99	736.54	734.1	0.26
18	$2s^22p^54s$	$^3P_1$	784.43	784.29	784.61	786.8398	0.32
19	$2s^22p^54s$	$^3P_0$	792.86	792.48	792.77	794.7816	0.29
20	$2s^22p^54s$	$^1P_1$	793.15	792.76	793.08	795.0707	0.29
21	$2s^22p^54p$	$^3S_1$	794.96	794.83	795.03	796.9821	0.27
22	$2s^22p^54p$	$^3P_1$	796.46	796.32	796.69	798.62	0.29
23	$2s^22p^54p$	$^3D_1$	805.28	804.09	805.23	806.332	0.28
24	$2s^22p^54d$	$^3P_0$	809.40	809.27	809.61	811.5967	0.29
25	$2s^22p^54d$	$^3P_1$	809.78	809.62	809.96	811.9451	0.29
26	$2s^22p^54d$	$^3D_1$	813.58	813.41	813.60	815.5056	0.26
27	$2s^22p^54f$	$^3D_1$	816.90	816.74	817.06	819.1565	0.30
28	$2s^22p^54d$	$^1P_1$	822.05	821.66	821.75	823.4	0.21

comprising $1s^22s^22p^6$, $1s^22s^22p^5nl$ (n = 3–10), $1s^22s2p^6nl$ (n = 3–10), and $1s^22s2p^53snl$ (n = 4–10), resulting in 260 fine-structure levels. For brevity and comparison with existing data, only those with total angular momentum $J = 0$ and 1 are presented in Table 1, while a complete set of the lowly excited energy levels is available from the Science Data Bank at https://www.scidb.cn/s/JFjQnm (https://doi.org/10.57760/sciencedb.j00113.00331). The listed levels follow the ordering of the NIST compilation of experimentally determined energies [78], with the ground

state $2s^2 2p^6$ $(^1S_0)^e$ serving as the zero-energy reference. The presently calculated results are compared with one another as well as with the data compiled by the NIST [78]. The relative deviations of the GRASP2K results from the NIST values are denoted by $\Delta\%$ in Table 1. The energy levels obtained from the three computational methods exhibit excellent agreement. Specifically, the present MCDHF results show maximum relative discrepancies of 0.20% with respect to the FAC values and 0.15% to the DARC values. Compared to the NIST reference data, the present MCDHF, FAC, and DARC results show maximum discrepancies of 0.51%, 0.44%, and 0.48%, respectively, as detailed in Table 1. The slight difference between the DARC and MCDHF deviations from the NIST values may be attributed to the distinct treatments of radial integrals and relativistic effects. The consistency of the energy levels and wave functions of Cr^{14+} ions obtained from the MCDHF approach with existing results confirms their convergence and reliability, justifying their subsequent use in the cross-section calculations. The validity of the $n = 4$ model for photoionization calculations is further supported by convergence studies on ions with comparable electronic structures in similar photon energy ranges, and by the expected isoelectronic trends in cross-section magnitude and resonance density [75–77].

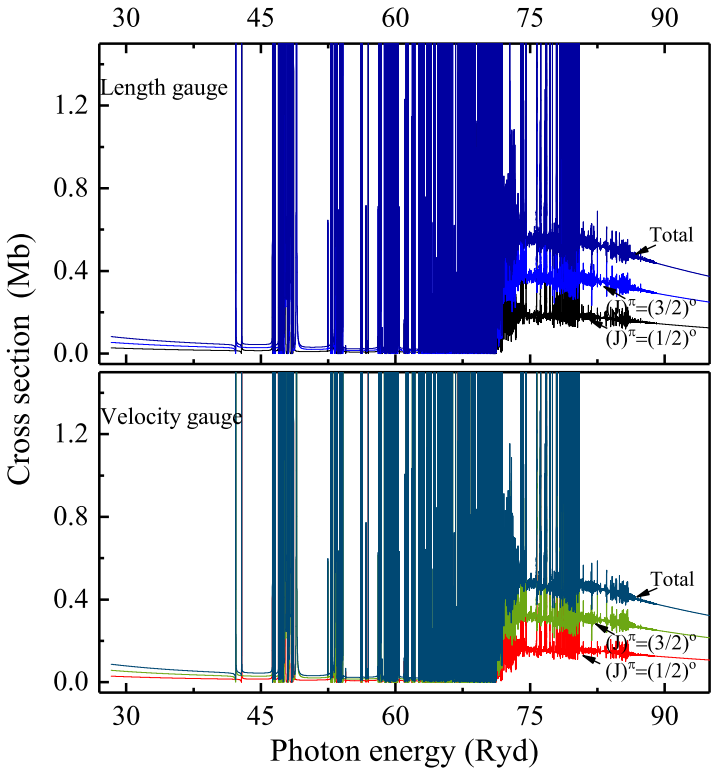


Figure 1: Photoionization cross sections for direct and resonant processes from the ground state $1s^2 2s^2 2p^6 3s$ $(^2S_{1/2})^e$ of Na-like Cr^{13+} ions, shown in the length gauge (top panel) and velocity gauge (bottom panel).

Fig. 1 shows the cross sections for the direct and resonant photoionization from the ground state [Ne]$3s$ $(^2S_{1/2})^e$ of Na-like Cr^{13+} ions. The results for the $(J)^\pi = (1/2)^o$ and $(3/2)^o$ resonance channels from intermediate doubly-excited states are plotted separately in the length gauge (top panel) and velocity gauge (bottom panel). Under both gauges, the cross sections for the resonance channel $(J)^\pi = (3/2)^o$ significantly exceed those for the $(J)^\pi = (1/2)^o$ one, a difference dominated by the statistical weight factor, with minor contributions from dynamical effects. Under the constraints of the E1 selection rule governed by total angular momentum and parity conservation, the ionizing light excites Cr^{13+} ions into only both the channels from the ground state $(J)^\pi = (1/2)^e$. Therefore, the total photoionization cross sections are obtained by summing the contributions from both the channels, as shown in the figure. The direct ionization limit of Cr^{13+} is determined to be 28.34 Ryd, being consistent with the corresponding NIST value of 28.2354 Ryd. This agreement further supports the validity of the present photoionization cross-section data. The relative deviations between the length and velocity gauge results for the photoionization cross sections do not exceed 14% for nearly all photon energies. In particular, the two gauges exhibit good agreement in the low-to-intermediate photon energy region and across the dominant resonance peaks. Given this consistency, hereafter, we focus exclusively on the results calculated within the length gauge. When using the cross sections at high photon energies, we recommend that the difference between the two gauge results be regarded as an estimate of the inherent theoretical uncertainty. The total photoionization cross sections obtained for both gauges are retrievable from the Science Data Bank at https://www.scidb.cn/s/JFjQnm (https://doi.org/10.57760/sciencedb.j00113.00331).

Figure 2 presents the total photoionization cross sections obtained with the length gauge, aiming to identify the resonance ionization limits of Cr^{13+} ions. The resonance peaks are found to be closely spaced across photon energies ranging from 42 to 86 Ryd, whereas at higher energies they become relatively sparse and the corresponding cross sections level off. For this reason, calculations at photon energies beyond this range were not pursued in the present study. As indicated by black arrows in the figure, several abrupt variations in the otherwise smooth photoionization continuum originate from the series limits of distinct Rydberg series. For illustration, the resonance ionization limit of 71.30 Ryd is derived as the sum of the excitation threshold (42.96 Ryd) for the $2p^5 3s\ ^3P_1$ level and the direct ionization limit of 28.34 Ryd. Notably, this resonance ionization limit corresponds exactly to the direct ionization limit of the $2p^5 3s\ ^3P_1$ level of neighboring Cr^{14+} ions. This equivalence stems from the fact that a Rydberg series limit of Cr^{13+} ions corresponds to the outermost electron occupying a state with such a high principal quantum number n that it is effectively at infinity. Hence, the energy levels of Cr^{14+} ions serve as reliable benchmarks for the Rydberg series limits of Cr^{13+}

Table 2: Resonance ionization limits for the ground-state resonant photoionization of Na-like Cr^{13+} ions, defined by the energy levels of Cr^{14+} ions.

Index	Energy level	Ionization limit (Ryd)
1	$2p^5 3s\ ^3P_1$	71.30
2	$2p^5 3s\ ^3P_0$	71.83
3	$2p^5 3p\ ^1S_0$	73.93
4	$2s2p^6 3s\ ^1S_0$	80.50
5	$2p^5 4s\ ^3P_1$	86.02

ions. Several additional ionization limits are also identified and labeled in Fig. 2, while the relevant energy levels used to designate these limits are listed in Table 2. It should be noted that further ionization limits also lie near these energy levels. However, they can not be separately resolved due to their close spacing and partial overlap.

The resonant doubly-excited states of Na-like Cr^{13+} ions are analyzed in detail by performing accurate energy-level calculations with the FAC package, where the reference configurations include all those with $n \leq 15$. By comparing these FAC energy levels with the resonance peak positions extracted from the cross sections computed using the DARC, the dominant resonant photoionization channels are identified. As illustrated in Fig. 2, the resonance peaks originating from distinct or identical Rydberg series exhibit a high density distribution across the photon energy range of 42–86 Ryd, which overlap partially or even completely, making it impossible to identify them individually. Indeed,

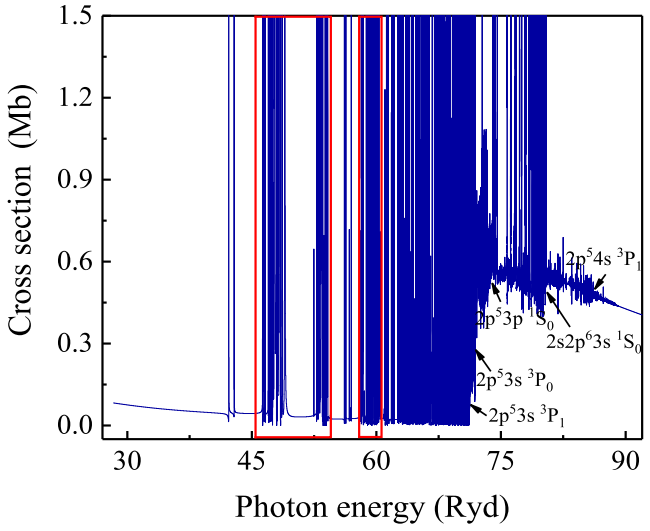


Figure 2: Total photoionization cross sections (length gauge) for direct and resonant processes from the ground state $1s^2 2s^2 2p^6 3s\ (^2S_{1/2})^e$ of Cr^{13+} ions, as a function of photon energy.

these resonance peaks are so sharp that their relevant Rydberg series converge quickly to their respective series limits, which inevitably leads to extensive resonance peak overlap [81, 82]. This overlapping structure is directly driven by channel coupling [83], and the critical role of relativistic effects in generating complex resonance structures has been established even for low-Z ions [84]. From a theoretical standpoint, the overlapping

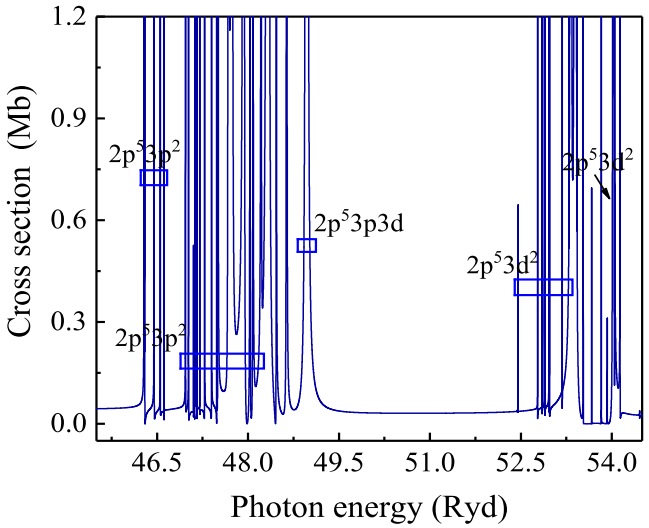


Figure 3: Same as Fig. 2 but for the ionizing photon energy range of 45.5–54.5 Ryd.

Table 3: Resonance channels and associated resonant energies for those peaks assigned in the ground-state photoionization of Na-like Cr^{13+} ions over the ionizing photon energy range of 45.5–54.5 Ryd.

Index	Resonance channel	Photon energy (Ryd)
1	$2p^5 3p^2\,(J)^\pi = (3/2)^o$	46.29
2	$2p^5 3p^2\,(J)^\pi = (1/2)^o$	46.46
3	$2p^5 3p^2\,(J)^\pi = (3/2)^o$	46.54
4	$2p^5 3p^2\,(J)^\pi = (3/2)^o$	46.96
5	$2p^5 3p^2\,(J)^\pi = (1/2)^o$	47.12
6	$2p^5 3p^2\,(J)^\pi = (3/2)^o$	47.30
7	$2p^5 3p^2\,(J)^\pi = (1/2)^o$	48.02
8	$2p^5 3p3d\,(J)^\pi = (1/2)^e$	48.91
9	$2p^5 3p3d\,(J)^\pi = (3/2)^e$	49.03
10	$2p^5 3d^2\,(J)^\pi = (3/2)^o$	52.45
11	$2p^5 3d^2\,(J)^\pi = (3/2)^o$	52.78
12	$2p^5 3d^2\,(J)^\pi = (1/2)^o$	52.83
13	$2p^5 3d^2\,(J)^\pi = (1/2)^o$	52.97
14	$2p^5 3d^2\,(J)^\pi = (3/2)^o$	53.18
15	$2p^5 3d^2\,(J)^\pi = (3/2)^o$	54.03

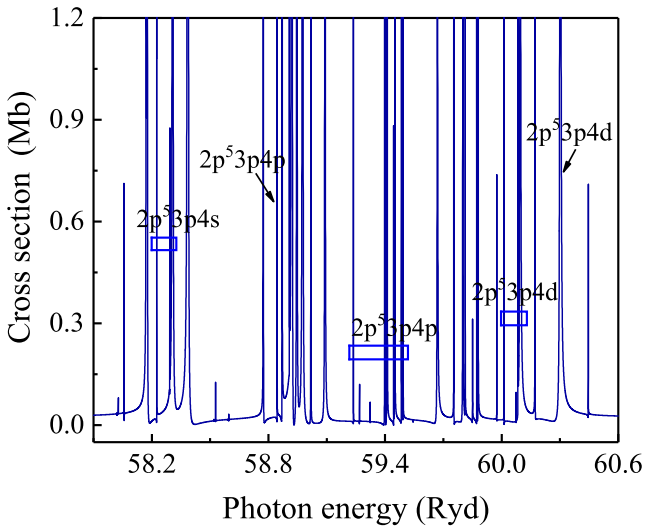


Figure 4: Same as Fig. 2 but for the ionizing photon energy range of 57.9–60.6 Ryd.

Rydberg series can thus be attributed to relativistic intermixing and channel coupling [85]. Because the resonance peaks are so closely spaced that they are difficult to resolve individually, we zoom in on the cross sections over the photon energy ranges of 45.5–54.5 and 57.9–60.6 Ryd (as indicated by the red box in Fig. 2), for which the peaks become sparse enough to be clearly distinguished. By matching the energy levels of Na-like Cr^{13+} ions with the resonance positions extracted from the photoionization cross sections, we identify 25 relatively well-separated resonance peaks at the level of electron configuration or even fine structure. These assignments are explicitly displayed in enlarged views in Figs. 3 and 4, while the corresponding energies are tabulated respectively in Tables 3 and 4. As an illustrative example, the resonance peak at 46.29 Ryd is identified as the level $2p^5 3p^2\,(J)^\pi = (3/2)^o$. As the photon energy increases, the resonance peaks become so densely packed that they cannot be identified even at the electron-configuration level.

In addition to the ground-state photoionization of Cr^{13+} ions, we also examine the direct and resonant photoionization from two lowly excited states $[\mathrm{Ne}]3p\ ^2P_{1/2,\,3/2}$. Fig. 5 illustrates the associated total photoionization cross sections calculated within the length gauge. As is the case for the ground state, the total photoionization cross sections for both the lowly excited states are available from the Science Data Bank at https://www.scidb.cn/s/JFjQnm (https://doi.org/10.57760/sciencedb.j00113.00331), which are presented for both the gauges and all the ionizing photon energies considered. Notably, the resonance structures associated with the two excited states closely resemble those obtained for the ground state. The direct ionization limits of the states $[\mathrm{Ne}]3p\ ^2P_{1/2}$ and $[\mathrm{Ne}]3p\ ^2P_{3/2}$ are determined to be 26.07 and 25.95 Ryd, respectively. These results exhibit excellent concordance with the values of 26.0238 and 25.8984 Ryd from the NIST [78], with respective discrepancies of only 0.18% and 0.20%. Determining the resonant

Table 4: The same as Table 3, but for the photon energy range of 57.9–60.6 Ryd.

Index	Resonance channel	Photon energy (Ryd)
1	$2p^5 3p4s\,(J)^\pi = (1/2)^e$	58.22
2	$2p^5 3p4s\,(J)^\pi = (3/2)^e$	58.29
3	$2p^5 3p4p\,(J)^\pi = (1/2)^o$	58.84
4	$2p^5 3p4p\,(J)^\pi = (1/2)^o$	59.24
5	$2p^5 3p4p\,(J)^\pi = (1/2)^o$	59.41
6	$2p^5 3p4p\,(J)^\pi = (3/2)^o$	59.45
7	$2p^5 3p4p\,(J)^\pi = (1/2)^o$	59.49
8	$2p^5 3p4d\,(J)^\pi = (1/2)^e$	60.01
9	$2p^5 3p4d\,(J)^\pi = (3/2)^e$	60.09
10	$2p^5 3p4d\,(J)^\pi = (1/2)^e$	60.30

ionization limits and identifying the resonance peaks for excited states proves much more challenging compared with those for the ground state. The extreme density of peaks and the inherently complex resonance structure essentially render any detailed investigation infeasible. Nevertheless, the systematic photoionization data and theoretical analyses obtained in this study, which cover ground- and excited-state photoionization processes of Na-like Cr^{13+} ions, are expected to facilitate diagnostic interpretation and numerical simulation of pertinent astrophysical and laboratory plasmas, complementing existing datasets of other chromium ions.

4. Conclusions

In summary, a systematic theoretical study of photoionization of Na-like Cr^{13+} from its ground state $1s^2 2s^2 2p^6 3s\ ^2S_{1/2}$ and two lowly excited states $1s^2 2s^2 2p^6 3p\ ^2P_{1/2,\,3/2}$ was carried out by employing the R-matrix theory and the MCDHF approach. Energy levels of Cr^{13+} and Cr^{14+} ions were obtained by means of three computational schemes (i.e., the DARC, FAC, and GRASP2K). The obtained results agree well with the NIST values. The generated wave functions were then used as input for the DARC to compute the direct and resonant photoionization cross sections over a broad span of photon energies with fine energy steps. For the ground-state photoionization, we identified 25 relatively well-resolved resonance peaks at the level of electron configuration or even fine structure by matching the calculated energy levels with the resonance positions extracted from the cross sections. These peaks were found to stem from the resonance channels $1s^2 2s^2 2p^5 3lnl'$ $(l = p, d)$. As for the excited states, however, the resonance peaks were so structurally complex and densely spaced that neither individual peaks nor the resonant ionization limits could be identified, despite the availability of the

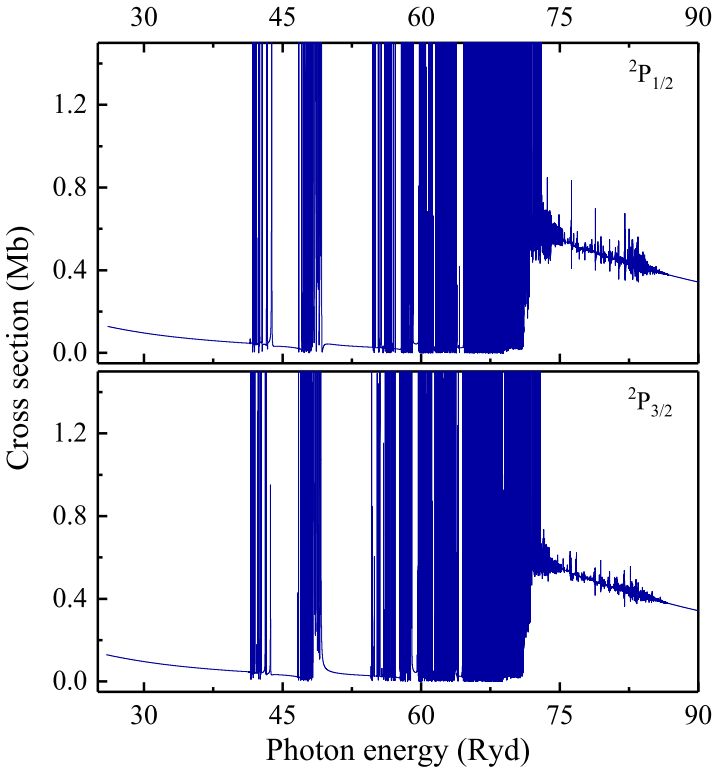


Figure 5: Same as Fig. 2 but for direct and resonant photoionization of Na-like Cr^{13+} ions from their lowly excited states [Ne]$3p\ ^2P_{1/2}$ and $^2P_{3/2}$.

direct ionization limits. The present work addresses the gap in the direct and resonant photoionization studies of Na-like Cr^{13+} ions and also provides a comprehensive set of photoionization cross-section data, which is retrievable from the Science Data Bank at https://www.scidb.cn/s/JFjQnm (https://doi.org/10.57760/sciencedb.j00113.00331). Along with other relevant datasets, these results are expected to facilitate diagnostic analysis and numerical simulation of chromium-containing astrophysical and laboratory plasmas and also advance a broader understanding of dynamical effects in highly charged iron-group ions.

Data availability

The data that support the findings of this study are openly available in the Science Data Bank at https://www.scidb.cn/s/JFjQnm (https://doi.org/10.57760/sciencedb.j00113.00331).

Acknowledgments

This work has been funded by the National Natural Science Foundation of China under Grants No. 12574281 and No. 12174315, the Outstanding Youth Fund of the

Science and Technology Project of Gansu Province under Grant No. 23JRRA687, and the Special Doctoral Program of the Youth Science and Technology Talent Cultivation Project from the China Association for Science and Technology in 2025.

References

[1] Mahla S and Antony B 2024 *Mon. Not. R. Astron. Soc.* **533** 2048–2057

[2] Gao J W, Han X Y, Wang J G and Li J M 2015 *Mon. Not. R. Astron. Soc.* **454** 315–321

[3] Stancalie V 2018 *J. Quant. Spectrosc. Radiat. Transfer* **205** 7–18

[4] Stancalie V 2021 *J. Quant. Spectrosc. Radiat. Transfer* **260** 107437

[5] Liang G Y, Li F, Wang F L, Wu Y, Zhong J Y and Zhao G 2014 *Astrophys. J.* **783** 124

[6] Sakho I, Tine M, Dieng M, Diop B, Faye M, Sow M, Guèye M, Biaye M and Wagué A 2014 *Radiat. Phys. Chem.* **101** 8–14

[7] Bautista M A, Lind K and Bergemann M 2017 *Astron. Astrophys.* **606** A127

[8] Dunleavy N L, Ballance C P, Ramsbottom C A and Jeffery C S 2021 *Mon. Not. R. Astron. Soc.* **506** 5398–5409

[9] Fernández-Menchero L, Jeffery C S, Ramsbottom C A and Ballance C P 2020 *Mon. Not. R. Astron. Soc.* **496** 2558–2564

[10] Zheng X F, Chen X H, Chen Y Y, Dong B L, Zhang K, Yao G X and Cui Z F 2012 *J. Chem. Phys.* **136** 174304

[11] Ayari T, Desouter-Lecomte M, Linguerri R, Garcia G A, Nahon L, Houria A B, Ghalila H, Said R B and Hochlaf M 2020 *Adv. Phys. X* **5** 1831955

[12] Belova O M and Bychkov K V 2018 *Astrophysics* **61** 224–240

[13] Bouziane A and Djebli M 2025 *Adv. Space Res.* **76** 6975–6984

[14] Dors Jr O L, Cardaci M V, Hägele G F and Krabbe Â C 2014 *Mon. Not. R. Astron. Soc.* **443** 1291–1300

[15] Keating L C, Haehnelt M G, Becker G D and Bolton J S 2013 *Mon. Not. R. Astron. Soc.* **438** 1820–1831

[16] Nicholls D C, Sutherland R S, Dopita M A, Kewley L J and Groves B A 2017 *Mon. Not. R. Astron. Soc.* **466** 4403–4422

[17] Fitzgerald K, Harvey E J, Keaveney N and Redman M P 2020 *Astron. Comput.* **32** 100382

[18] Chen Z B 2025 *Eur. Phys. J. Plus* **140** 782

[19] Singh A K, Dawra D, Dimri M, Jha A, Sharma R and Mohan M 2020 *Radiat. Phys. Chem.* **168** 108447

[20] Trzhaskovskaya M B and Nikulin V K 2014 *At. Data Nucl. Data Tables* **100** 986–1058

[21] Li M X, Wang H Y, Tahouri R, Weissenbilder R, Li J L, Wang W T, Cai J A, Hong X C, Shi X, Pi L W, Busto D, Gisselbrecht M, Ueda K, Demekhin P V, L'Huillier A, Dahlström J M, Lindroth E, Ding D and Luo S 2025 *Phys. Rev. Lett.* **135** 183202

[22] Petrov I D, Lagutin B M, Sukhorukov V L, Knie A and Ehresmann A 2016 *Phys. Rev. A* **93** 033408

[23] Lagutin B M, Petrov I D, Sukhorukov V L, Demekhin P V, Knie A and Ehresmann A 2017 *Phys. Rev. A* **95** 063414

[24] Hasoglu M F, Gorczyca T W and Manson S T 2021 *Phys. Scr.* **96** 124024

[25] Turck-Chièze S, Pennec M L, Ducret J E, Colgan J, Kilcrease D P, Fontes C J, Magee N, Gilleron F and Pain J C 2016 *Astrophys. J.* **823** 78

[26] Bäckström E, Gurell J, Royen P, Mannervik S, Norlin L, Blackwell-Whitehead R, Hartman H and Nilsson H 2012 *Mon. Not. R. Astron. Soc.* **420** 1636–1639

[27] Palmeri P, Deprince J, Bautista M A, Fritzsche S, Garcia J A, Kallman T R, Mendoza C and Quinet P 2022 *Astron. Astrophys.* **657** A61

[28] Engstrom L, Lundberg H, Nilsson H, Hartman H and Backstrom E 2014 *Astron. Astrophys.* **570** A34

[29] Chen Z B 2026 *J. Quant. Spectrosc. Radiat. Transfer* **348** 109706

[30] Yigit M and Tel E 2017 *Nucl. Sci. Tech.* **28** 165

[31] Lv S Q, Han W J, Yu J G, Zhou H, Liu M, Chen C A and Zhu K G 2018 *Chin. Phys. Lett.* **35** 126101

[32] Lagoyannis A, Tsavalas P, Mergia K, Provatas G, Triantou K, Tsompopoulou E, Rubel M, Petersson P, Widdowson A, Harissopulos S, Mertzimekis T and the JET contributors 2017 *Nucl. Fusion* **57** 076027

[33] Aharonian F, Akamatsu H, Akimoto F *et al.* 2017 *Nature* **551** 478

[34] Wallace L and Hinkle K 2009 *Astrophys. J.* **700** 720

[35] Lawler J E, Sneden C, Nave G, Hartog E A D, Emrahoğlu N and Cowan J J 2017 *Astrophys. J. Suppl. Ser.* **228** 10

[36] Bergemann M and Cescutti G 2010 *Astron. Astrophys.* **522** A9

[37] Tian Y, Wang X, Yu Q, Wang Q and Chen Z 2021 *J. Quant. Spectrosc. Radiat. Transf.* **274** 107880

[38] Flanagan J C, Sertoli M, Bacharis M, Matthews G F, de Vries P C, Widdowson A, Coffey I H, Arnoux G, Sieglin B, Brezinsek S, Coenen J W, Marsen S, Craciunescu T, Murari A, Harting D, Cackett A, Hodille E and Contributors J E 2014 *Plasma Phys. Control. Fusion* **57** 014037

[39] Rajput M, Vala S, Subhash P, Srinivasan R, Kumar R and Abhangi M 2018 *Fusion Eng. Des.* **130** 114–121

[40] Singh A, Dimri M, Dawra D, Jha A K S and Mohan M 2019 *Can. J. Phys.* **97** 436–442

[41] Peacock N J, Stamp M F and Silver J D 1984 *Phys. Scr.* **T8** 10

[42] Kumar N, Shivankar, Jha A K S, Dimri M, Dawra D and Mohan M 2023 *Eur. Phys. J. Plus* **138** 1155

[43] Konan G G and Özdemir L 2016 *Can. J. Phys.* **94** 1167–1174

[44] Staiger H, Mondeel G, Blundell S A, Dipti, O'Neil G, Silwal R, Lapierre A, Gwinner G, Tan J N, Gillaspy J D, Ralchenko Y and Takacs E 2025 *Phys. Rev. A* **112**(1) 012807

[45] Paijwar R and Sharma R 2023 *Eur. Phys. J. Plus* **138**(12) 1120

[46] Dzifčáková E, Dufresne R P, Dudík J and Del Zanna G 2024 *Astron. Astrophys.* **690** A340

[47] Safronova U, Safronova A and Beiersdorfer P 2009 *At. Data Nucl. Data Tables* **95**(6) 751–785

[48] Shen B F, Xu Z Z and Zhang W Q 1991 *Acta Opt. Sin.* **11**(9) 848

[49] Singh A, Dimri M, Dawra D, Jha A, Verma N and Mohan M 2019 *Radiat. Phys. Chem.* **156** 174–192

[50] He W L, Xie L Y, Niu S B, Rui J L, Ma Y L and Dong C Z 2025 *At. Data Nucl. Data Tables* **164** 101718

[51] Keskinen J, Huttula S M, Mäkinen A, Patanen M and Huttula M 2015 *Radiat. Phys. Chem.* **117** 209–216

[52] Mäkinen A, Niskanen J and Aksela H 2012 *Phys. Rev. A* **85**(5) 053411

[53] Nahar S N 2009 *J. Quant. Spectrosc. Radiat. Transf.* **110**(18) 2148–2161

[54] Zatsarinny O and Tayal S 2020 *Atoms* **8**(3) 51

[55] Ziegler M, Rauch T, Werner K, Köppen J and Kruk J W 2012 *Astron. Astrophys.* **548** A109

[56] De Cia A, Ledoux C, Fox A J, Vreeswijk P M, Smette A, Petitjean P, Björnsson G, Fynbo J P U, Hjorth J and Jakobsson P 2012 *Astron. Astrophys.* **545** A64

[57] Ben-Yami M, Madhusudhan N, Cabot S H C, Constantinou S, Piette A, Gandhi S and Welbanks L 2020 *Astrophys. J. Lett.* **897**(1) L5

[58] West J B, Hansen J E, Kristensen B, Folkmann F and Kjeldsen H 2003 *J. Phys. B: At. Mol. Opt. Phys.* **36**(19) L327

[59] Wang H B 2022 *Indian J. Phys.* **96**(13) 3743–3753

[60] Yadav F, Goyal A, Singh N and Mohan M 2024 *Indian J. Phys.* **98**(5) 1573–1582

[61] Limandri S P, Carreras A C, Trincavelli J C, Guzmán J A, Mitnik D M, Montanari C C and Segui S 2025 *At. Data Nucl. Data Tables* **166** 101756

[62] Aggarwal S, Singh J and Mohan M 2013 *At. Data Nucl. Data Tables* **99**(6) 704–732

[63] Biémont E, Frémat Y and Quinet P 1999 *At. Data Nucl. Data Tables* **71**(1) 117–146

[64] Grant I P 2007 *Relativistic Quantum Theory of Atoms and Molecules: Theory and Computation* (New York: Springer)

[65] Wigner E P and Eisenbud L 1947 *Phys. Rev.* **72**(1) 29–41

[66] Burke P G, Hibbert A and Robb W D 1971 *J. Phys. B: At. Mol. Opt. Phys.* **4**(2) 153

[67] Chang J J 1975 *J. Phys. B: At. Mol. Opt. Phys.* **8**(14) 2327

[68] Norrington P H 2004 Dirac Atomic R-matrix Codes

[69] Li Y, Wang J Q and Wu Z W 2025 *J. Phys. B: At. Mol. Opt. Phys.* **58**(14) 145001

[70] Wang J Q, Li Y and Wu Z W 2025 *Phys. Plasmas.* **32**(9) 093301

[71] An Y H, Wu Z W, Jiang J, Xie L Y, Zhang D H and Dong C Z 2021 *J. Phys. B: At. Mol. Opt. Phys.* **54**(6) 065001

[72] Norrington P H and Grant I P 1981 *J. Phys. B: At. Mol. Opt. Phys.* **14**(7) L261

[73] Liang J, Han M, Liao Y, Ji J, Leung C S, Jiang W, Ueda K, Zhou Y, Lu P and Wörner H J 2024 *Nat. Photon.* **18**(4) 311–317

[74] Berrington K A, Eissner W B and Norrington P H 1995 *Comput. Phys. Commun.* **92**(2) 290–420

[75] Sardar S, Bilal M, Nazir R T, Bari M A, Hannan A and Nasim M H 2015 *Mon. Not. R. Astron. Soc.* **450**(2) 1631–1637

[76] Singh A K, Dawra D, Dimri M, Jha A K S and Mohan M 2019 *Eur. Phys. J. D* **73**(5) 85

[77] Tyndall N B, Ramsbottom C A, Ballance C P and Hibbert A 2016 *Mon. Not. R. Astron. Soc.* **456**(1) 366–373

[78] Sugar J and Corliss C 1985 *J. Phys. Chem. Ref. Data* **14**(2) 664

[79] Gu M F 2008 *Can. J. Phys.* **86**(5) 675–689

[80] Jönsson P, He X, Fischer C and Grant I P 2007 *Comput. Phys. Commun.* **177**(7) 597–622

[81] Kim D S and Kwon D H 2015 *J. Phys. B: At. Mol. Opt. Phys.* **48**(10) 105004

[82] Singh A K, Dimri M, Dawra D, Jha A and Mohan M 2019 *J. Phys. B: At. Mol. Opt. Phys.* **52**(7) 075002

[83] Scott N S and Burke P G 1980 *J. Phys. B: At. Mol. Phys.* **13**(21) 4299

[84] Xie L Y, Man Q Q, Wang J G, Qu Y Z and Dong C Z 2018 *Chin. Phys. B* **27**(8) 083201

[85] Khatri I, Goyal A, Aggarwal S, Singh A and Mohan M 2015 *Can. J. Phys.* **93**(11) 1221–1226